THE JOURNAL OF PHYSICAL CHEMISTRY Letters

pubs.acs.org/JPCL

Letter

Strain and Charge Doping Fingerprints of the Strong Interaction between Monolayer MoS_2 and Gold

Matěj Velický,* Alvaro Rodriguez, Milan Bouša, Andrey V. Krayev, Martin Vondráček, Jan Honolka, Mahdi Ahmadi, Gavin E. Donnelly, Fumin Huang, Héctor D. Abruña, Kostya S. Novoselov, and Otakar Frank*

Cite This: *J. Phys. Chem. Lett.* 2020, 11, 6112–6118

Read Online

ACCESS | Metrics & More | Article Recommendations | Supporting Information

ABSTRACT: Gold-mediated exfoliation of MoS_2 has recently attracted considerable interest. The strong interaction between MoS_2 and Au facilitates preferential production of centimeter-sized monolayer MoS_2 with near-unity yield and provides a heterostructure system noteworthy from a fundamental standpoint. However, little is known about the detailed nature of the MoS_2–Au interaction and its evolution with the MoS_2 thickness. Here, we identify the specific vibrational and binding energy fingerprints of this interaction using Raman and X-ray photoelectron spectroscopy, which indicate substantial strain and charge doping in monolayer MoS_2. Tip-enhanced Raman spectroscopy reveals heterogeneity of the MoS_2–Au interaction at the nanoscale, reflecting the spatial nonconformity between the two materials. Micro-Raman spectroscopy shows that this interaction is strongly affected by the roughness and cleanliness of the underlying Au. Our results elucidate the nature of the MoS_2–Au interaction and guide strain and charge doping engineering of MoS_2.

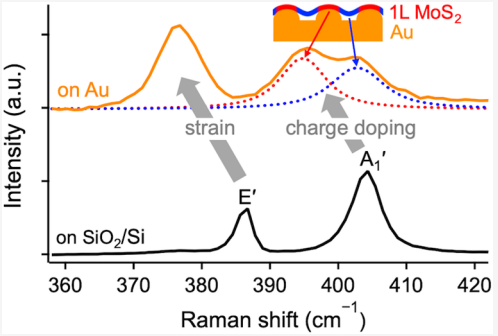

Several groups have recently introduced a method of exfoliating large-area transition metal dichalcogenide monolayers using gold substrates or sacrificial layers.[1−3] For MoS_2 in particular, it is possible to prepare centimeter-sized monolayers, thanks to their preferential near-unity exfoliation yield and the high quality of natural molybdenite.[3] This is a major advancement for mechanical exfoliation, which produces the highest-quality crystals but has been challenging to scale up, unlike the readily scalable chemical vapor deposition (CVD) or liquid phase-exfoliation that produces lower-quality crystals. Gold-mediated exfoliation has quickly attracted attention and has been utilized in the fabrication of flexible gas sensors,[4] lithography patterning for transistor applications,[5] and construction of large-area van der Waals (vdW) heterostructures.[6,7]

When bulk MoS_2 is pressed against freshly deposited Au and peeled off, monolayer MoS_2 crystals with a near-unity yield remain on the Au surface.[2,3] This was rationalized theoretically, showing that the binding energy between the bottom-most MoS_2 layer and Au is larger than the interlayer equivalent in bulk MoS_2,[3] and that the biaxial strain induced in MoS_2 facilitates preferential monolayer exfoliation in the naturally AB-stacked molybdenite (2H phase in Ramsdell notation).[8] It was suggested that the MoS_2–Au interaction is of vdW rather than covalent nature, and that when the Au is removed, the optical and electronic properties of monolayer MoS_2 match those of the semiconducting 1H phase, exfoliated directly onto insulating substrates.[2,3,5,6] This signifies that the metallicity of MoS_2 endowed by the Au[3,9] can be reversed after its transfer onto another substrate, significantly increasing the scope of this method to optoelectronics, photovoltaics, and photocatalysis. Despite these efforts, little is known about the nature of the interaction between MoS_2 and Au, its dependence on the number of MoS_2 layers, and specific effects brought about in MoS_2.

Here, we study the interaction between MoS_2 and Au using Raman spectroscopy and X-ray photoelectron spectroscopy (XPS). MoS_2 was mechanically exfoliated on a range of polycrystalline Au substrates with thicknesses of 3–100 nm, prepared by magnetron sputtering, electron-beam (e-beam) evaporation, and thermal evaporation (see the Methods section in the Supporting Information for details). Monolayer (1L), bilayer (2L), trilayer (3L), and bulk MoS_2 crystals were readily identified due to their high optical contrast,[10] as demonstrated in Figure 1a. The far-field micro-Raman spectra of 1L MoS_2 on Au exhibit conspicuous broadening and downshift of the E′ mode and splitting of the A_1' mode, in

Received: April 28, 2020
Accepted: July 7, 2020
Published: July 7, 2020

https://dx.doi.org/10.1021/acs.jpclett.0c01287
J. Phys. Chem. Lett. 2020, 11, 6112–6118

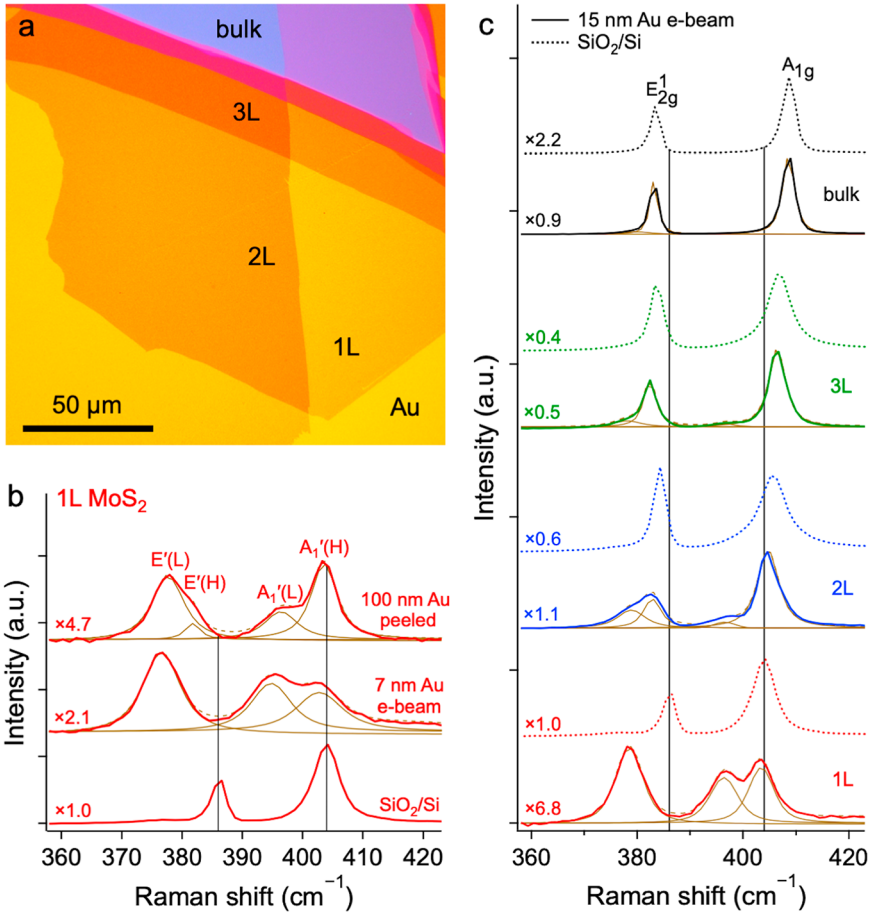

Figure 1. Micro-Raman spectra of MoS_2 on Au. (a) Optical image of MoS_2 exfoliated on Au (15 nm e-beam). (b) Raman spectra of monolayer MoS_2 on different substrates: SiO_2/Si, 7 nm e-beam Au, and 100 nm thermal Au peeled from Si. (c) Raman spectra of 1L, 2L, 3L, and bulk MoS_2 on 15 nm e-beam Au (solid) and SiO_2/Si (dotted). Spectra were collected using a 532 nm excitation and normalized to their highest peaks with the corresponding multiplicators shown on the left. Curve fittings using the Voigt function are shown in brown.

comparison to 1L MoS_2 on SiO_2/Si (Figure 1b). Lattice deformation (strain) and charge transfer (doping) are the two main factors influencing Raman frequencies in 1L MoS_2.[11] The effect of lateral strain is more pronounced for the in-plane E′ phonon,[12,13] while charge doping has a greater influence on the out-of-plane A_1' phonon.[14,15] The E′ mode broadening and downshift can thus be interpreted as heterogeneous biaxial strain, originating in the lattice mismatch between MoS_2 and Au.[16,17] The induced change in the frequency of a generic Raman mode M can be estimated as $\delta\omega_M = \omega_M^0 - \omega_M = 2\gamma_M\omega_M^0\varepsilon$, where ω_M^0 and ω_M are the Raman frequencies of the M mode in unstrained and strained lattices, respectively, γ_M is the Grüneisen parameter of the M mode, and ε is the biaxial strain.[11]

Since the precise values of zero-strain Raman frequencies in 1L MoS_2 ($\omega_{E'}^0$ and $\omega_{A_1'}^0$) are unknown, we use $\omega_{E'}^{SiO_2/Si}$ = (385.9 ± 0.2) cm^{-1} measured on SiO_2/Si as a reference. The E′ mode peak frequency for all the 1L MoS_2/Au samples in this study averages at $\omega_{E'}$ = (378.2 ± 0.6) cm^{-1}, which yields $\delta\omega_{E'}$ = 7.7 cm^{-1} and implies a tensile strain of ε = (1.2 ± 0.1)% when $\gamma_{E'}$ = 0.82 is used (average from refs 11 and 12). If the observed broadening of the E′ mode on Au with a line width of $\Gamma_{E'}$ = (6.1 ± 0.5) cm^{-1} were caused solely by heterogeneous lattice deformation, the biaxial tension would fall between 0.6% and 1.9%, taken as the 5th and 95th percentiles of the distribution of peaks with $\Gamma_{E'}$ = 2.4 cm^{-1} (as measured on SiO_2/Si) within the broadened E′ peak.

The average strain-induced downshift of the A_1' mode should be $\delta\omega_{A_1'}$ = (1.7 ± 0.2) cm^{-1}, calculated using ε = 1.2%, $\omega_{A_1'}^{SiO_2/Si}$ = (404.0 ± 0.2) cm^{-1}, and $\gamma_{A_1'}$ = 0.18.[11,12] However, the A_1' mode is visibly split into two components (Figure 1b), which we define as the lower-frequency A_1'(L) mode at (396.4 ± 0.3) cm^{-1} and the higher-frequency A_1'(H) mode at (403.7 ± 0.2) cm^{-1}, corresponding to $\delta\omega_{A_1'(L)}$ = 7.6 cm^{-1} and $\delta\omega_{A_1'(H)}$ = 0.3 cm^{-1}. The most probable origin of the highly downshifted A_1'(L) component is the substrate-induced doping, which affects a portion of the 1L MoS_2. The net A_1'(L) shift $\delta\omega_{A_1'(L)}^{corr}$ = 5.9 cm^{-1}, corrected for the strain by subtracting 1.7 cm^{-1}, implies n-type doping and the electron concentration estimate of $n_e \sim 2.6 \times 10^{13}$ cm^{-2} for A_1'(L).[14,18] Conversely, the strain-corrected net A_1'(H) shift, $\delta\omega_{A_1'(H)}^{corr}$ = −1.4 cm^{-1}, points to an electron withdrawal. Since the SiO_2/Si reference is known to induce n-doping in MoS_2,[19,20] this suggests that A_1'(H) corresponds to regions of undoped MoS_2 without direct contact with Au. The dominant n-type doping of MoS_2 induced by the Au was confirmed independently by estimating the MoS_2−Au work function difference (ΔΦ) from the ultraviolet photoelectron spectroscopy (UPS) as ∼0.3 eV and from Kelvin probe force microscopy (KPFM) as ∼0.2 eV (Figures S1 and S2, respectively). The small difference in ΔΦ

https://dx.doi.org/10.1021/acs.jpclett.0c01287
J. Phys. Chem. Lett. 2020, 11, 6112−6118

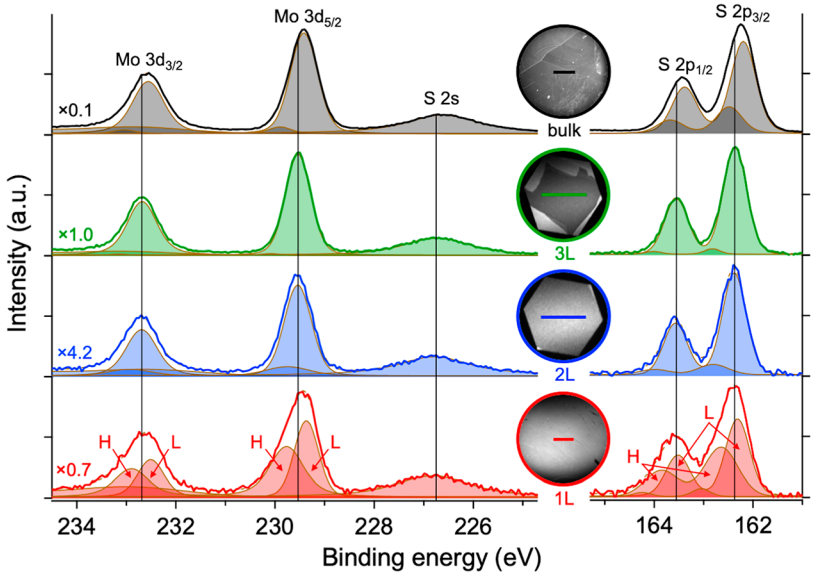

Figure 2. Micro-XPS of MoS_2 on Au. Mo 3d (left) and S 2p (right) core-level spectra for 1L, 2L, 3L, and bulk MoS_2 on Au (15 nm e-beam). Normalization and fitting, qualitatively similar to that in Figure 1, were applied. The insets show the PEEM images of the measured areas with 30 μm scale bars.

determined by these two techniques can be attributed to the environmental effects of the adsorbed moisture and/or oxygen in the case of KPFM, which was performed in the ambient.[21]

The broadening and splitting of the E′ and A_1' Raman modes suggest that the MoS_2–Au interaction is heterogeneous, leading to a multitude of strain and doping states of the MoS_2, manifested in the convoluted multicomponent spectral response in Figure 1b,c. In the extreme case of the top spectrum in Figure 1b (100 nm Au peeled), the dominating low-frequency component E′(L) is accompanied by a high-frequency shoulder E′(H), the presence of which is correlated with the A_1'(H) intensity, as discussed below.

The evolution of the Raman spectra with the number of MoS_2 layers shown in Figure 1c for the Au (15 nm e-beam) and SiO_2/Si substrates brings further clarity. It transpires that only the bottom-most MoS_2 layer interacts strongly with the adjacent Au substrate, while the top layers in 2L, 3L, and bulk MoS_2, without a direct contact with Au, are only partially strained and virtually undoped (see also Figure 4a). We arrive at this conclusion since E′(L) and A_1'(L) are replicated in the thicker layers also, with their frequencies and absolute intensities maintained. These components are readily resolved in 2L, less so in 3L, and negligible in bulk, due to the increased intensities of E′(H) and A_1'(H) (Figure 1c). Note that the notation of the Raman modes in MoS_2 is layer-dependent due to symmetry considerations. Thus, E′ and A_1' versus E^1_{2g} and A_{1g} irreducible representations are used for an odd number of layers versus even number of layers and bulk.[22]

The observed strain and doping are among the highest observed to date.[9,12,14,15,18,23−25] Several previous studies of the MoS_2/Au heterostructure report the Raman spectra. Upshifts of both the E′/E^1_{2g} and A_1'/A_{1g} modes with the MoS_2 thickness were observed using a low-resolution spectrometer,[3,10] consistent with Figure 1c if heavily averaged spectra are considered. A broadening and downshift of E′ due to strain and upshift of A_1' explained by out-of-plane vibration stiffening were observed for 1L CVD MoS_2 with the Au deposited on top,[16] contradicting the appearance of A_1'(L) in our study. A downshift of E′ assigned to strain and an undiscussed low-frequency component near A_1' were reported recently.[9,13] A similar behavior of both the E′ and A_1' modes to that in our work was observed in 1L CVD MoS_2 grown on single-crystal Au(111) but was interpreted as an out-of-plane strain[26] arising from the moiré heterostructure buckling due to the MoS_2/Au lattice mismatch.[17]

Figure 2 shows the micro-XPS data for the Mo 3d and S 2p core levels, obtained from 1L, 2L, 3L, and bulk MoS_2. Care was taken to minimize the effects of edges in 1L, which were shown to induce splitting of Mo 3d core levels.[27] Photoemission electron microscopy (PEEM) images of the sampled areas are shown in the insets. The Mo 3d and S 2p peaks in 1L are asymmetric, and their fitting with two Voigt doublets yields a good match with the spectra, revealing a chemical shift of ∼0.4 eV between the higher (H) and lower (L) binding energy components, which appear to have the same origin as A_1'(L) and A_1'(H) in the 1L Raman spectra (Figure 1b,c), respectively. The upshift (downshift) of H (L) in 1L from the dominant L component in 2L and 3L (vertical lines) reflects the Fermi level upshift (downshift) in 1L MoS_2 due to electron injection (withdrawal). This provides further evidence of the suspected heterogeneity of the MoS_2–Au interaction, with the MoS_2 n-doped when in contact with the Au (H) and undoped when detached from the Au (L). The H components are also partially replicated in the thicker layers, in analogy to A_1'(L) in the Raman spectra of Figure 1c.

The core-level peak energies in bulk MoS_2 are less reliable and burdened by larger uncertainties stemming from the weak Au $4f_{7/2}$ signal used as an internal calibration reference, effects of finite probing depth and charging, and presence of step-edges.[28] Importantly, despite the observed shifts in the XPS binding energies and Raman frequencies, the spectral responses are fully consistent with the thermodynamically stable semiconducting 1H phase of 1L MoS_2,[3,9] rather than the unstable metallic 1T′ phase observed elsewhere.[29,30] This important conclusion demonstrates that the lattice symmetry of 1L MoS_2 is preserved and that the Au-induced metallicity can be fully reversed after a transfer onto an insulating substrate.[2,5]

https://dx.doi.org/10.1021/acs.jpclett.0c01287
J. Phys. Chem. Lett. 2020, 11, 6112−6118

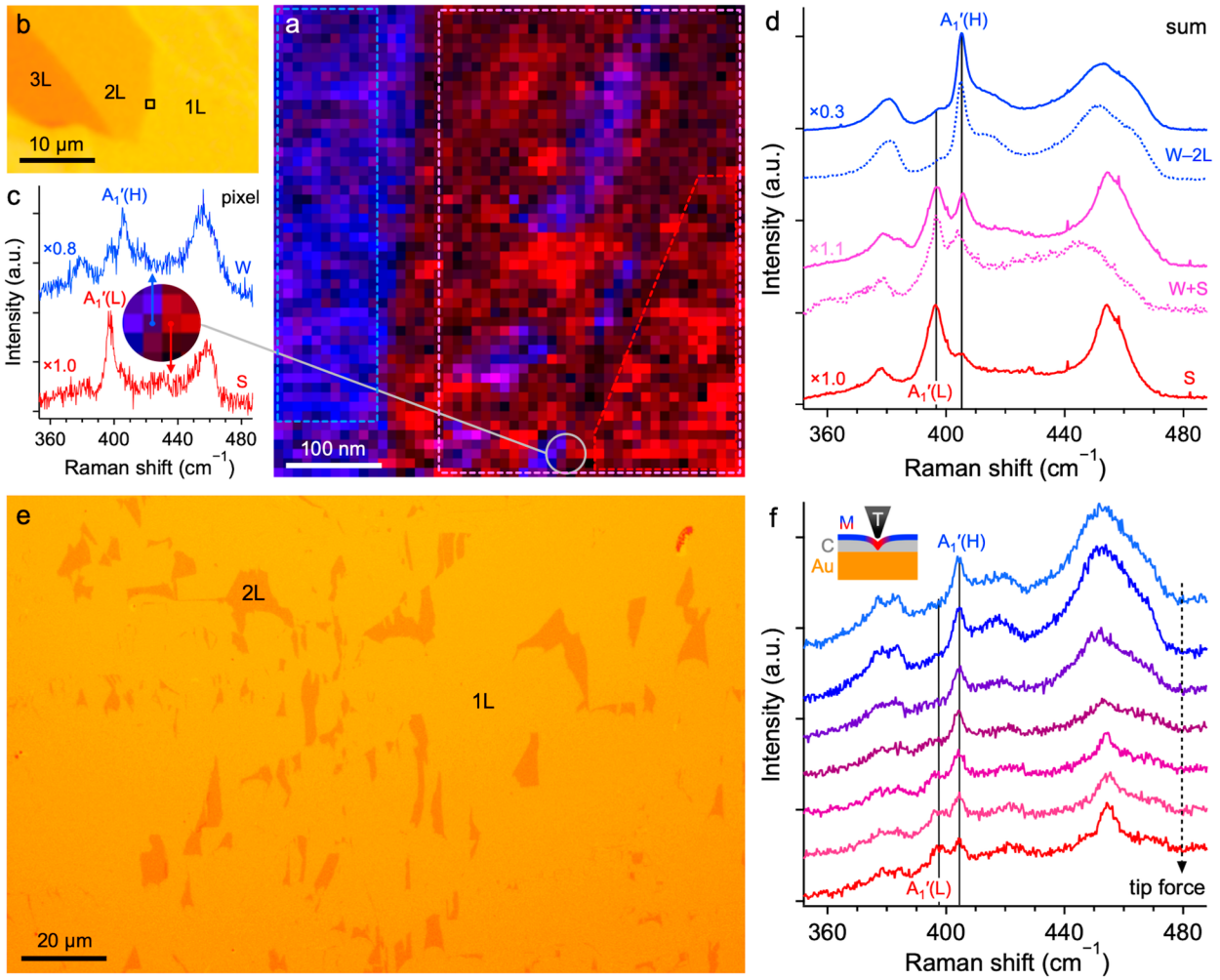

Figure 3. Tip-enhanced Raman spectroscopy of MoS_2 on Au. (a) TERS map (633 nm excitation) of an interface between 1L and 2L. Red, blue, and magenta hues correspond to the intensities of $A_1'(L)$, $A_1'(H)$, and both components, respectively. (b) Optical image of MoS_2 on Au (50 nm e-beam) with the TERS map area defined by a black rectangle. (c) Single-pixel (10 × 10) nm^2 TERS of the adjacent strongly (S) and weakly (W) interacting 1L MoS_2. (d) TERS summed over the weakly interacting 2L (W−2L), strongly interacting 1L (S), and mixed regions (S+W), from areas highlighted in panel a by dashed polygons of matching colors. Corresponding micro-Raman spectra (633 nm excitation) are shown as dotted curves. (e) Optical image of microscale 2L inclusions in 1L MoS_2. (f) TERS acquired with a variable tip force to alter the MoS_2−Au interaction. The inset illustrates how the tip (T) pushes the MoS_2 (M) closer to the Au through a layer of contamination (C).

Figure 3a shows the near-field tip-enhanced Raman spectroscopy (TERS) mapping of an area in Figure 3b, which allowed us to isolate the $A_1'(L)$ and $A_1'(H)$ components of the Raman spectra of 1L MoS_2 on Au. The spectra of two individual adjacent (10 × 10) nm^2 pixels shown in Figure 3c differ greatly and correspond to 1L MoS_2 strongly (S in red) and weakly (W in blue) interacting with the Au. The S spectrum features only $A_1'(L)$, while the W spectrum is dominated by $A_1'(H)$ with a small $A_1'(L)$ shoulder. The blue patches in a larger red region in the right-hand portion of Figure 3a therefore indicate the presence of weakly interacting nanoscale inclusions in a strongly interacting 1L MoS_2 sheet. TERS signals summed over the pure weakly interacting bilayer (W−2L), pure strongly interacting monolayer (S), and mixed (S+W) regions of the map, shown as solid curves in Figure 3d, corroborate this conclusion. The mixed response in particular (magenta) is in excellent agreement with the micro-Raman spectrum (dotted curve) recorded in the same area. Unreliability of the absolute intensities in fast TERS mapping makes the differentiation between signals from 2L and weakly interacting 1L challenging. We therefore cannot rule out the disruption of the preferential 1L exfoliation by a locally weakened MoS_2−Au interaction, potentially leading to nanoscale traces of 2L. Indication of such a phenomenon, with 2L inclusions in a continuous sheet of 1L, was occasionally observed at the microscale (Figure 3e).

However, a direct proof of the 1L origin of $A_1'(L)$ is provided by a series of TERS measurements in Figure 3f, acquired using a variable tip force on 1L MoS_2 transferred onto 50 nm Au using a polydimethylsiloxane stamp. As no attention was paid to the freshness and cleanliness of the MoS_2 and Au surfaces in this case, a layer of contamination was trapped between the two materials, through which we pushed the TERS tip to alter their separation. The top spectrum in Figure 3f corresponds to the weakly interacting 1L MoS_2/Au with $A_1'(H)$ present but $A_1'(L)$ missing. As the tip force increases, and the MoS_2 is pressed against the Au (Figure 3f, inset), their interaction is strengthened, and $A_1'(L)$ begins to appear at the expense of the $A_1'(H)$ intensity. The fact the $A_1'(L)$ and $A_1'(H)$ modes show no frequency change also proves that no

https://dx.doi.org/10.1021/acs.jpclett.0c01287
J. Phys. Chem. Lett. 2020, 11, 6112−6118

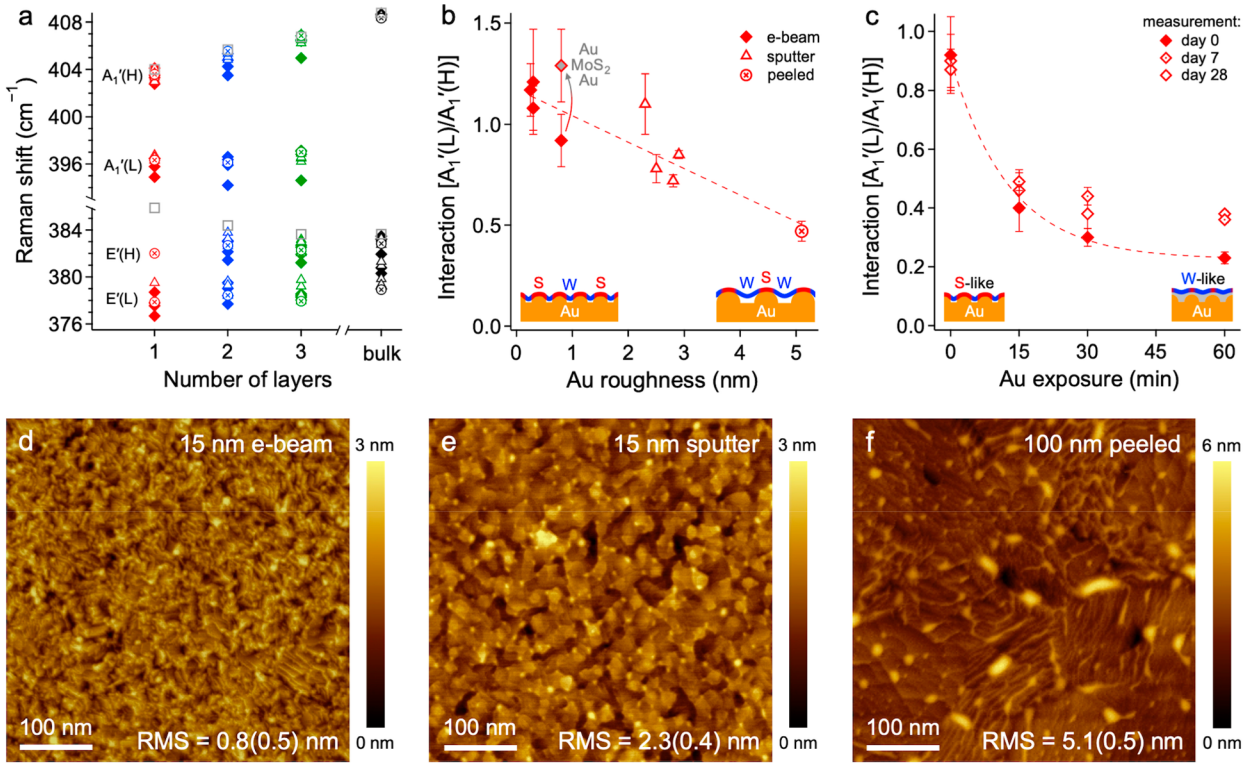

Figure 4. Correlation between surface structure and Raman vibrations of MoS_2. (a) Raman frequencies as a function of the number of MoS_2 layers for all samples. (b) $A_1'(L)/A_1'(H)$ as a function of the Au roughness, determined by AFM. In comparison, the average roughness of 1L MoS_2 was (0.4 ± 0.1) nm. The gray-filled marker corresponds to the 5 nm Au/1L MoS_2/15 nm Au "sandwich". (c) $A_1'(L)/A_1'(H)$ as a function of the Au exposure to air prior to the MoS_2 exfoliation (0, 15, 30, 60 min), measured at different times after sample preparation (day 0, 7, 28). Diamond, triangle, circle, and square markers in panels a–c, obtained using the Voigt fitting of the micro-Raman spectra (532 nm excitation), denote the e-beam Au, sputtered Au, peeled Au, and SiO_2/Si substrates, respectively. (d–f) AFM images of 1L MoS_2 on 15 nm e-beam, 15 nm sputter, and 100 nm peeled Au, respectively, noting the root-mean-square roughness (RMS) of the Au (MoS_2) surface.

measurable strain is induced by the tip compression.[31] On the contrary, the only changing parameter is the relative intensity of the two A_1' components, indicating that an increasingly larger area of MoS_2 interacts electronically with the Au.

Figure 4a details the evolution of the E'/E^1_{2g} and A_1'/A_{1g} frequencies with the number of MoS_2 layers determined by micro-Raman for all the Au (color) and SiO_2/Si (gray) substrates. The $A_1'(H)$ component on Au upshifts with an increasing number of layers the same way A_1'/A_{1g} does on SiO_2/Si.[32,33] In contrast, the $A_1'(L)$ component maintains its frequency for 1L–3L, which makes evident its origin in the strongly interacting regions of the bottom-most MoS_2 layer. Figure 4b shows that the ratio between the $A_1'(L)$ and $A_1'(H)$ intensities of 1L MoS_2 [$A_1'(L)/A_1'(H)$], which is proportional to the strength of the MoS_2–Au interaction, strongly correlates with the Au roughness determined by atomic force microscopy (AFM). This supports the intuitive expectation that the increased conformity of MoS_2 to smoother Au increases the strength of their interaction (Figure 4b, insets). In Figure 4c, we show that $A_1'(L)/A_1'(H)$ decreases exponentially with the time of Au exposure to air prior to the MoS_2 exfoliation. This further makes evident the weakening of the MoS_2–Au interaction due to airborne contamination (see Figure 4c, insets), in agreement with the observed suppression of the initially near-unity 1L yield after 15–20 min of Au exposure to air.[3] For the freshly made Au (0 min), $A_1'(L)/A_1'(H)$ does not depend on the time delay between the Raman measurement and MoS_2 exfoliation (day 0 to day 28). In contrast, $A_1'(L)/A_1'(H)$ slightly increases with the time delay for the aged Au (15–60 min), indicating that the contact between MoS_2 and contaminated Au improves with time.

AFM images of the 1L MoS_2/Au heterostructure in Figure 4d–f show signs of MoS_2 being suspended between the nanocrystalline features on the Au surface, with a good (poor) contact at the protrusions (depressions). As the Au roughness increases, a larger portion of MoS_2 becomes decoupled from the substrate, leading to an increased intensity of the weakly interacting $A_1'(H)$ (Figure 4b, insets). A larger portion of weakly interacting, suspended MoS_2 also leads to a relative increase in the $E'(H)$ intensity, as seen for the roughest Au substrate (top spectrum in Figure 1b). The enhancement of the MoS_2–Au interaction through an increased contact area is further made evident by the Au/MoS_2/Au "sandwich" made by covering 1L MoS_2 on 15 nm Au with another layer of 5 nm Au, leading to a 40% increase in $A_1'(L)/A_1'(H)$ indicated by the gray-filled marker in Figure 4b.

The wide range of Au thicknesses (3–100 nm) and roughnesses (0.3–5.1 nm) prepared by three different techniques makes evident the fact that the strong MoS_2–Au interaction and the resulting near-unity 1L MoS_2 exfoliation yield are universal, as long as the surfaces are kept clean. Polycrystallinity of our Au also disproves the previous suggestion that only single-crystal Au(111) exhibits the strong interaction with MoS_2.[26] This, along with the fact that both the exfoliation and characterization are performed in the ambient environment, and not limited to ultrahigh vacuum conditions, opens this research up to a broad scientific community.

https://dx.doi.org/10.1021/acs.jpclett.0c01287
J. Phys. Chem. Lett. 2020, 11, 6112–6118

The novel experimental evidence in this study unequivocally links the appearance of the downshifted $A_1'(L)$ Raman mode to that portion of 1L MoS_2, which strongly interacts with the Au substrate. The n-doping of 1L MoS_2 in contact with Au, proven by XPS, UPS, and KPFM, corroborates that it is the increased electron concentration which is responsible for the $A_1'(L)$ downshift, in line with electrochemically gated MoS_2 experiments.[14,15,18] Nevertheless, one could envisage alternative explanations. The strong binding in MoS_2−Au heterostructures with a clean interface could cause softening of the Mo−S bonds,[26] instead of the stiffening seen for the contaminated MoS_2−Au interface.[16] The MoS_2−Au interaction could also lead to activation of phonons otherwise silent in 1L MoS_2, such as those present in multilayer systems.[33,34] However, this can be ruled out for $A_1'(L)$, since an activation of another mode would not lead to a disappearance of the original A_1', observed in our TERS data. Furthermore, we observed the same apparent splitting of A_1' into $A_1'(L)$ and $A_1'(H)$ in the micro-Raman spectra of 1L WS_2 on Au, with the $A_1'(L)$ downshifted by ∼7 cm^{-1} (Figure S3). This is a nearly identical shift to that for 1L MoS_2, which points to an electron density increase rather than activation of a new mode.

In summary, we identify the specific vibrational and binding energy fingerprints of the strong interaction between MoS_2 and Au. Raman spectroscopy reveals significant downshift and broadening of the in-plane E′ mode of 1L MoS_2 on Au, compared to MoS_2 on SiO_2/Si, arising from heterogeneous biaxial tensile strains of up to 1.9%. Splitting of the out-of-plane A_1' Raman mode and XPS Mo 3d and S 2p core levels into two separate components implies that a portion of MoS_2 is in close contact with the Au and experiences n-type charge doping with electron concentrations up to 2.6×10^{13} cm^{-2}, while another portion is suspended and undoped. The evolution of the spectra with the MoS_2 thickness confirms that the MoS_2−Au interaction is confined to the bottom-most MoS_2 layer. TERS mapping confirms the nanoscale heterogeneity of this interaction caused by the spatial nonconformity between the two materials. Finally, we show that the MoS_2−Au interaction can be effectively tuned by the surface roughness and cleanliness of the underlying Au substrate, which could be exploited for strain and charge doping engineering of MoS_2.

■ ASSOCIATED CONTENT

Supporting Information

The Supporting Information is available free of charge at https://pubs.acs.org/doi/10.1021/acs.jpclett.0c01287.

Methods; work function estimation from UPS; work function estimation from KPFM; and Raman spectra of 1L WS_2 on Au (PDF)

■ AUTHOR INFORMATION

Corresponding Authors

Matěj Velický − *Department of Physics and Astronomy, University of Manchester, Manchester M13 9PL, United Kingdom; Department of Chemistry and Chemical Biology, Cornell University, Ithaca, New York 14853, United States; School of Mathematics and Physics, Queen's University Belfast, Belfast BT7 1NN, United Kingdom;* orcid.org/0000-0003-4230-3811; Email: matej.velicky@manchester.ac.uk

Otakar Frank − *J. Heyrovský Institute of Physical Chemistry, Czech Academy of Sciences, 182 23 Prague, Czech Republic;* orcid.org/0000-0002-9661-6250; Email: otakar.frank@jh-inst.cas.cz

Authors

Alvaro Rodriguez − *J. Heyrovský Institute of Physical Chemistry, Czech Academy of Sciences, 182 23 Prague, Czech Republic*

Milan Bouša − *J. Heyrovský Institute of Physical Chemistry, Czech Academy of Sciences, 182 23 Prague, Czech Republic;* orcid.org/0000-0002-1073-7386

Andrey V. Krayev − *HORIBA Scientific, Novato, California 94949, United States*

Martin Vondráček − *Institute of Physics, Czech Academy of Sciences, 182 21 Prague 8, Czech Republic*

Jan Honolka − *Institute of Physics, Czech Academy of Sciences, 182 21 Prague 8, Czech Republic*

Mahdi Ahmadi − *Department of Chemistry and Chemical Biology, Cornell University, Ithaca, New York 14853, United States*

Gavin E. Donnelly − *School of Mathematics and Physics, Queen's University Belfast, Belfast BT7 1NN, United Kingdom*

Fumin Huang − *School of Mathematics and Physics, Queen's University Belfast, Belfast BT7 1NN, United Kingdom;* orcid.org/0000-0001-6489-9818

Héctor D. Abruña − *Department of Chemistry and Chemical Biology, Cornell University, Ithaca, New York 14853, United States;* orcid.org/0000-0002-3948-356X

Kostya S. Novoselov − *Department of Physics and Astronomy, University of Manchester, Manchester M13 9PL, United Kingdom; Centre for Advanced 2D Materials, National University of Singapore, 117546, Singapore; Chongqing 2D Materials Institute, Chongqing 400714, China*

Complete contact information is available at: https://pubs.acs.org/10.1021/acs.jpclett.0c01287

Notes

The authors declare no competing financial interest.

■ ACKNOWLEDGMENTS

This project has received funding from the European Union's Horizon 2020 research and innovation program under the Marie Skłodowska-Curie grant agreement No. 746685, EPSRC grant No. EP/N025938/1, and the Czech Science Foundation project GACR 17-18702S. This work was performed in part at the Cornell NanoScale Science & Technology Facility, a member of the National Nanotechnology Coordinated Infrastructure, which is supported by the NSF (Grant NNCI-1542081), and made use of the Cornell Center for Materials Research Shared Facilities, which are supported through the NSF MRSEC program (DMR-1719875). This work was supported by the Ministry of Education, Youth and Sports of the Czech Republic (MEYS), and The European Union—European Structural and Investments Funds in the frame of Operational Programme Research Development and Education project Pro-NanoEnviCz (Reg. CZ.02.1.01/0.0/0.0/16_013/0001821). Photoemission spectroscopy experiments were supported by the MEYS of the Czech Republic through project CZ.02.1.01/0.0/0.0/16_013/0001406.

■ REFERENCES

(1) Magda, G. Z.; Pető, J.; Dobrik, G.; Hwang, C.; Biró, L. P.; Tapasztó, L. Exfoliation of Large-Area Transition Metal Chalcogenide Single Layers. *Sci. Rep.* **2015**, *5*, 14714.

(2) Desai, S. B.; Madhvapathy, S. R.; Amani, M.; Kiriya, D.; Hettick, M.; Tosun, M.; Zhou, Y.; Dubey, M.; Ager, J. W.; Chrzan, D.; et al. Gold-Mediated Exfoliation of Ultralarge Optoelectronically-Perfect Monolayers. *Adv. Mater.* **2016**, *28*, 4053−4058.
(3) Velický, M.; Donnelly, G. E.; Hendren, W. R.; McFarland, S.; Scullion, D.; DeBenedetti, W. J. I.; Correa, G. C.; Han, Y.; Wain, A. J.; Hines, M. A.; et al. Mechanism of Gold-Assisted Exfoliation of Centimeter-Sized Transition-Metal Dichalcogenide Monolayers. *ACS Nano* **2018**, *12*, 10463−10472.
(4) Guo, S.; Yang, D.; Li, B.; Dong, Q.; Li, Z.; Zaghloul, M. E. *2019 IEEE 62nd International Midwest Symposium on Circuits and Systems*, 4−7 Aug. 2019; pp 884−887.
(5) Gramling, H. M.; Towle, C. M.; Desai, S. B.; Sun, H.; Lewis, E. C.; Nguyen, V. D.; Ager, J. W.; Chrzan, D.; Yeatman, E. M.; Javey, A.; et al. Spatially Precise Transfer of Patterned Monolayer WS_2 and MoS_2 with Features Larger than 10^4 μm^2 Directly from Multilayer Sources. *ACS Appl. Electron. Mater.* **2019**, *1*, 407−416.
(6) Nguyen, V.; Gramling, H.; Towle, C.; Li, W.; Lien, D.-H.; Kim, H.; Chrzan, D. C.; Javey, A.; Xu, K.; Ager, J.; et al. Deterministic Assembly of Arrays of Lithographically Defined WS_2 and MoS_2 Monolayer Features Directly From Multilayer Sources Into Van Der Waals Heterostructures. *J. Micro Nano-Manuf.* **2019**, *7*, 041006.
(7) Liu, F.; Wu, W.; Bai, Y.; Chae, S. H.; Li, Q.; Wang, J.; Hone, J.; Zhu, X.-Y. Disassembling 2D van der Waals crystals into macroscopic monolayers and reassembling into artificial lattices. *Science* **2020**, *367*, 903−906.
(8) Sun, H.; Sirott, E. W.; Mastandrea, J.; Gramling, H. M.; Zhou, Y.; Poschmann, M.; Taylor, H. K.; Ager, J. W.; Chrzan, D. C. Theory of thin-film-mediated exfoliation of van der Waals bonded layered materials. *Phys. Rev. Mater.* **2018**, *2*, 094004.
(9) Blue, B. T.; Jernigan, G. G.; Le, D.; Fonseca, J. J.; Lough, S. D.; Thompson, J. E.; Smalley, D. D.; Rahman, T. S.; Robinson, J. T.; Ishigami, M. Metallicity of 2H-MoS_2 induced by Au hybridization. *2D Mater.* **2020**, *7*, 025021.
(10) Donnelly, G. E.; Velický, M.; Hendren, W. R.; Bowman, R. M.; Huang, F. Achieving extremely high optical contrast of atomically-thin MoS_2. *Nanotechnology* **2020**, *31*, 145706.
(11) Michail, A.; Delikoukos, N.; Parthenios, J.; Galiotis, C.; Papagelis, K. Optical detection of strain and doping inhomogeneities in single layer MoS_2. *Appl. Phys. Lett.* **2016**, *108*, 173102.
(12) Lloyd, D.; Liu, X.; Christopher, J. W.; Cantley, L.; Wadehra, A.; Kim, B. L.; Goldberg, B. B.; Swan, A. K.; Bunch, J. S. Band Gap Engineering with Ultralarge Biaxial Strains in Suspended Monolayer MoS_2. *Nano Lett.* **2016**, *16*, 5836−5841.
(13) Pető, J.; Dobrik, G.; Kukucska, G.; Vancsó, P.; Koós, A. A.; Koltai, J.; Nemes-Incze, P.; Hwang, C.; Tapasztó, L. Moderate strain induced indirect bandgap and conduction electrons in MoS_2 single layers. *npj 2D Mater. Appl.* **2019**, *3*, 39.
(14) Chakraborty, B.; Bera, A.; Muthu, D. V. S.; Bhowmick, S.; Waghmare, U. V.; Sood, A. K. Symmetry-dependent phonon renormalization in monolayer MoS_2 transistor. *Phys. Rev. B: Condens. Matter Mater. Phys.* **2012**, *85*, 161403.
(15) Melnikova-Kominkova, Z.; Jurkova, K.; Vales, V.; Drogowska-Horná, K.; Frank, O.; Kalbac, M. Strong and efficient doping of monolayer MoS_2 by a graphene electrode. *Phys. Chem. Chem. Phys.* **2019**, *21*, 25700−25706.
(16) Gong, C.; Huang, C.; Miller, J.; Cheng, L.; Hao, Y.; Cobden, D.; Kim, J.; Ruoff, R. S.; Wallace, R. M.; Cho, K.; et al. Metal Contacts on Physical Vapor Deposited Monolayer MoS_2. *ACS Nano* **2013**, *7*, 11350−11357.
(17) Sørensen, S. G.; Füchtbauer, H. G.; Tuxen, A. K.; Walton, A. S.; Lauritsen, J. V. Structure and Electronic Properties of In Situ Synthesized Single-Layer MoS_2 on a Gold Surface. *ACS Nano* **2014**, *8*, 6788−6796.
(18) Sohier, T.; Ponomarev, E.; Gibertini, M.; Berger, H.; Marzari, N.; Ubrig, N.; Morpurgo, A. F. Enhanced Electron-Phonon Interaction in Multivalley Materials. *Phys. Rev. X* **2019**, *9*, 031019.
(19) Scheuschner, N.; Ochedowski, O.; Kaulitz, A.-M.; Gillen, R.; Schleberger, M.; Maultzsch, J. Photoluminescence of freestanding single- and few-layer MoS_2. *Phys. Rev. B: Condens. Matter Mater. Phys.* **2014**, *89*, 125406.
(20) Rodriguez, A.; Verhagen, T.; Kalbac, M.; Vejpravova, J.; Frank, O. Imaging Nanoscale Inhomogeneities and Edge Delamination in As-Grown MoS_2 Using Tip-Enhanced Photoluminescence. *Phys. Status Solidi RRL* **2019**, *13*, 1900381.
(21) Konečný, M.; Bartošík, M.; Mach, J.; Švarc, V.; Nezval, D.; Piastek, J.; Procházka, P.; Cahlík, A.; Šikola, T. Kelvin Probe Force Microscopy and Calculation of Charge Transport in a Graphene/Silicon Dioxide System at Different Relative Humidity. *ACS Appl. Mater. Interfaces* **2018**, *10*, 11987−11994.
(22) Pimenta, M. A.; del Corro, E.; Carvalho, B. R.; Fantini, C.; Malard, L. M. Comparative Study of Raman Spectroscopy in Graphene and MoS_2-type Transition Metal Dichalcogenides. *Acc. Chem. Res.* **2015**, *48*, 41−47.
(23) Li, H.; Contryman, A. W.; Qian, X.; Ardakani, S. M.; Gong, Y.; Wang, X.; Weisse, J. M.; Lee, C. H.; Zhao, J.; Ajayan, P. M.; et al. Optoelectronic crystal of artificial atoms in strain-textured molybdenum disulphide. *Nat. Commun.* **2015**, *6*, 7381.
(24) Rice, C.; Young, R. J.; Zan, R.; Bangert, U.; Wolverson, D.; Georgiou, T.; Jalil, R.; Novoselov, K. S. Raman-scattering measurements and first-principles calculations of strain-induced phonon shifts in monolayer MoS_2. *Phys. Rev. B: Condens. Matter Mater. Phys.* **2013**, *87*, 081307.
(25) Trainer, D. J.; Zhang, Y.; Bobba, F.; Xi, X.; Hla, S.-W.; Iavarone, M. The Effects of Atomic-Scale Strain Relaxation on the Electronic Properties of Monolayer MoS_2. *ACS Nano* **2019**, *13*, 8284−8291.
(26) Yasuda, S.; Takahashi, R.; Osaka, R.; Kumagai, R.; Miyata, Y.; Okada, S.; Hayamizu, Y.; Murakoshi, K. Out-of-Plane Strain Induced in a Moiré Superstructure of Monolayer MoS_2 and $MoSe_2$ on Au(111). *Small* **2017**, *13*, 1700748.
(27) Bruix, A.; Füchtbauer, H. G.; Tuxen, A. K.; Walton, A. S.; Andersen, M.; Porsgaard, S.; Besenbacher, F.; Hammer, B.; Lauritsen, J. V. *In Situ* Detection of Active Edge Sites in Single-Layer MoS_2 Catalysts. *ACS Nano* **2015**, *9*, 9322−9330.
(28) Mattila, S.; Leiro, J. A.; Heinonen, M.; Laiho, T. Core level spectroscopy of MoS_2. *Surf. Sci.* **2006**, *600*, 5168−5175.
(29) Yu, Y.; Nam, G.-H.; He, Q.; Wu, X.-J.; Zhang, K.; Yang, Z.; Chen, J.; Ma, Q.; Zhao, M.; Liu, Z.; et al. High phase-purity 1T′-MoS_2- and 1T′-$MoSe_2$-layered crystals. *Nat. Chem.* **2018**, *10*, 638−643.
(30) Yin, X.; Wang, Q.; Cao, L.; Tang, C. S.; Luo, X.; Zheng, Y.; Wong, L. M.; Wang, S. J.; Quek, S. Y.; Zhang, W.; et al. Tunable inverted gap in monolayer quasi-metallic MoS_2 induced by strong charge-lattice coupling. *Nat. Commun.* **2017**, *8*, 486.
(31) Peña-Álvarez, M.; del Corro, E.; Morales-García, Á.; Kavan, L.; Kalbac, M.; Frank, O. Single Layer Molybdenum Disulfide under Direct Out-of-Plane Compression: Low-Stress Band-Gap Engineering. *Nano Lett.* **2015**, *15*, 3139−3146.
(32) Lee, C.; Yan, H.; Brus, L. E.; Heinz, T. F.; Hone, J.; Ryu, S. Anomalous Lattice Vibrations of Single- and Few-Layer MoS_2. *ACS Nano* **2010**, *4*, 2695−2700.
(33) Zhang, X.; Qiao, X.-F.; Shi, W.; Wu, J.-B.; Jiang, D.-S.; Tan, P.-H. Phonon and Raman scattering of two-dimensional transition metal dichalcogenides from monolayer, multilayer to bulk material. *Chem. Soc. Rev.* **2015**, *44*, 2757−2785.
(34) Scheuschner, N.; Gillen, R.; Staiger, M.; Maultzsch, J. Interlayer resonant Raman modes in few-layer MoS_2. *Phys. Rev. B: Condens. Matter Mater. Phys.* **2015**, *91*, 235409.

https://dx.doi.org/10.1021/acs.jpclett.0c01287
J. Phys. Chem. Lett. 2020, 11, 6112−6118